Phosphorylated claudin-16 interacts with Trpv5 and regulates transcellular calcium transport in the kidney

Jianghui Hou[a,1], Vijay Renigunta[b], Mingzhu Nie[c], Abby Sunq[a], Nina Himmerkus[d], Catarina Quintanova[d], Markus Bleich[d], Aparna Renigunta[e], and Matthias Tilmann Florian Wolf[c]

[a]Department of Internal Medicine – Renal Division, Washington University St. Louis, St. Louis, MO 63110; [b]Department of Neurophysiology, Institute of Physiology and Pathophysiology, University of Marburg, 35037 Marburg, Germany; [c]Department of Pediatrics, Pediatric Nephrology, University of Texas Southwestern Medical Center, Dallas, TX 75390; [d]Department of Physiology, University of Kiel, 24098 Kiel, Germany; and [e]University Children's Hospital, University of Marburg, 35037 Marburg, Germany

Edited by Martin R. Pollak, Beth Israel Deaconess Medical Center, Brookline, MA, and approved August 13, 2019 (received for review February 3, 2019)

Familial hypomagnesemia with hypercalciuria and nephrocalcinosis (FHHNC) was previously considered to be a paracellular channelopathy caused by mutations in the claudin-16 and claudin-19 genes. Here, we provide evidence that a missense FHHNC mutation c.908C>G (p.T303R) in the claudin-16 gene interferes with the phosphorylation in the claudin-16 protein. The claudin-16 protein carrying phosphorylation at residue T303 is localized in the distal convoluted tubule (DCT) but not in the thick ascending limb (TAL) of the mouse kidney. The phosphomimetic claudin-16 protein carrying the T303E mutation but not the wildtype claudin-16 or the T303R mutant protein increases the Trpv5 channel conductance and membrane abundance in human kidney cells. Phosphorylated claudin-16 and Trpv5 are colocalized in the luminal membrane of the mouse DCT tubule; phosphomimetic claudin-16 and Trpv5 interact in the yeast and mammalian cell membranes. Knockdown of claudin-16 gene expression in transgenic mouse kidney delocalizes Trpv5 from the luminal membrane in the DCT. Unlike wildtype claudin-16, phosphomimetic claudin-16 is delocalized from the tight junction but relocated to the apical membrane in renal epithelial cells because of diminished binding affinity to ZO-1. High-Ca^{2+} diet reduces the phosphorylation of claudin-16 protein at T303 in the DCT of mouse kidney via the PTH signaling cascade. Knockout of the PTH receptor, PTH1R, from the mouse kidney abrogates the claudin-16 phosphorylation at T303. Together, these results suggest a pathogenic mechanism for FHHNC involving transcellular Ca^{2+} pathway in the DCT and identify a molecular component in renal Ca^{2+} homeostasis under direct regulation of PTH.

tight junction | claudin | PTH | calcium | Trpv5

Familial hypomagnesemia with hypercalciuria and nephrocalcinosis (FHHNC; OMIM no. 248250) is a monogenic Mendelian disease first described by Michelis and colleagues (1). By linkage analysis and positional cloning, Simon and colleagues mapped FHHNC to chromosome 3q27 and identified the causal gene, claudin-16 (formerly known as paracellin-1) (2). The claudin-16 gene is highly expressed by the thick ascending limb (TAL) of the kidney, which handles ~25% of Ca^{2+} reabsorption and 70% of Mg^{2+} reabsorption via the paracellular pathway (3). Claudins are tetraspan membrane proteins consisting of a family of 28 members that form the paracellular channels to allow selective permeation of ions and solutes through the tight junction (TJ) (4). Hou and colleagues showed that claudin-16 is required for paracellular permeation of monovalent cations, e.g., Na^+, as well as divalent cations, e.g., Mg^{2+} and Ca^{2+}, in the TAL of mouse kidney (5). The claudin-16 gene has a substantial expression on the mRNA level in the distal convoluted tubule (DCT) of the kidney (2). The functional role of claudin-16 in the DCT, however, is completely unknown.

The Ca^{2+} reabsorption in the DCT is primarily handled by the Trpv5 channel (formerly known as ECaC1) via the transcellular pathway (6). Genetic ablation of Trpv5 in the mouse kidney caused severe hypercalciuria due to reduced Ca^{2+} reabsorption in the DCT (7). Despite strong functional evidence from cell and animal models, there is no Mendelian disease genetically linked to mutation in Trpv5. A few recent studies have identified nonsynonymous polymorphisms in the Trpv5 gene from various forms of hypercalciuria, including kidney stone disease, but no functional alteration can be attributed to these polymorphisms (8, 9). On the contrary, numerous mutations in claudin-16 have been found to cosegregate with FHHNC (2, 10). Among them, a missense mutation c.908C>G (p.T303R) affects the carboxyl-terminal PDZ-binding motif (-TRV) in claudin-16 important for its interaction with ZO-1, a TJ peripheral protein (11). Unlike with other claudin-16 mutations, patients with the T303R mutation showed childhood hypercalciuria and nephrocalcinosis but no significant disturbance in renal Mg^{2+} handling (11). Based upon these phenotypic observations, we hypothesize that the T303R mutation predominantly perturbs claudin-16's function in the DCT, which results in a Ca^{2+}-specific abnormality.

Results

Development of a Phosphorylated Claudin-16 Antibody. Simon et al. first reported a substantial expression of claudin-16 mRNA in the TAL and the DCT tubules from the rabbit kidney (2). We performed microdissection and manual sorting on the mouse kidney to collect individual nephron segments and quantified claudin-16 mRNA levels in these segments with real-time PCR (*SI Appendix*, Fig. S1*A*). The molecular identity of each nephron segment was verified by measuring the mRNA levels of known gene markers, e.g., Na-K-Cl cotransporter 2 (NKCC2), Na-Cl

Significance

Claudin is the core protein making the tight junction and the paracellular channel. Whether it may regulate the transcellular pathway is not known. Here, we have discovered that phosphorylated claudin-16 proteins are not localized in the tight junction but found in the luminal membrane of the distal tubular cells, where they facilitate the transcellular Ca^{++} permeation via Trpv5. This discovery not only resolves a longstanding mystery pertaining to the role of transcellular Ca^{++} pathway in the FHHNC syndrome, but also reveals a class of functional binding partners for Trp channels.

Author contributions: J.H. and M.T.F.W. designed research; J.H., V.R., M.N., A.S., N.H., C.Q., A.R., and M.T.F.W. performed research; J.H., V.R., M.B., A.R., and M.T.F.W. analyzed data; and J.H. wrote the paper.

The authors declare no conflict of interest.

This article is a PNAS Direct Submission.

Published under the PNAS license.

[1]To whom correspondence may be addressed. Email: jhou@wustl.edu.

This article contains supporting information online at www.pnas.org/lookup/suppl/doi:10.1073/pnas.1902042116/-/DCSupplemental.

Published online September 5, 2019.

cotransporter (NCC), and Trpv5 (*SI Appendix*, Fig. S1*B*). The claudin-16 mRNA levels were the highest in the TAL; the DCT expressed ∼32.7% of claudin-16 transcripts as the TAL; the proximal tubule (PT), the connecting tubule (CNT), and the collecting duct (CD) were without claudin-16 transcription (*SI Appendix*, Fig. S1*B*). The transcriptional profile of claudin-16 in the mouse kidney was similar to that in the human kidney (12). We have previously developed a claudin-16 antibody against the carboxyl-terminal domain (TETAKMYAVDTRV) in the mouse claudin-16 protein. Immunohistological analyses of wildtype and claudin-16–null mouse kidneys revealed that claudin-16 proteins were only expressed in the TAL of the kidney (*SI Appendix*, Fig. S2). We hypothesize that the threonine residue (T233 in mouse claudin-16; T303 in human claudin-16 due to the fact that human claudin-16 utilizes the M71 as its true start codon [13]) in the carboxyl-terminal PDZ-binding motif (-TRV) of claudin-16 protein is naturally phosphorylated, which escapes the detection by the antibodies that bind to the unphosphorylated form. We have therefore raised an antibody to detect the phosphorylated claudin-16 protein at amino acid locus T303 (termed CLDN16-P antibody). The anti–CLDN16-P antibody was made by immunizing rabbits against the phosphorylated peptide: AKMYAVD(pT)RV. The antiserum was cross-absorbed against the unphosphorylated peptide AKMYAVDTRV and purified by affinity chromatography (*Methods*). The regular claudin-16 antibody selectively recognized the unmodified peptide (AKMYAVDTRV), while the phosphorylated claudin-16 antibody selectively recognized the phosphorylated peptide at T303 [AKMYAVD(pT)RV; *SI Appendix*, Fig. S3*A*]. We then adapted a Percoll gradient centrifugal approach according to Doctor et al. to isolate the distal tubules from collagenase digested mouse kidneys (14). The kidney cortices were removed, minced, and digested by collagenase into short tubular segments and then subjected to centrifugation in a 25–55% Percoll gradient. The distal tubules (DTs) can be separated from the PT and the glomeruli (G; *SI Appendix*, Fig. S3*B*). Microscopic examination revealed that the DT fraction contained the TAL, the DCT, and the CNT/CD (*SI Appendix*, Fig. S3*C*). The membranes from the isolated DT fraction were lysed and blotted against anti-CLDN16 or anti-CLDN16-P antibody. The claudin-16 protein band and the phosphorylated claudin-16 protein band were selectively lost in claudin-16–null mouse DT membranes (*SI Appendix*, Fig. S3*D*). Treatment with λ-phosphatase reduced the CLDN16-P signals, indicating that the DT cells contained phosphorylated claudin-16 proteins (*SI Appendix*, Fig. S3*E*). Together, these results establish the specificity of the antibody for phosphorylated claudin-16 (T303-P).

Phosphorylated Claudin-16 Protein Is Localized in the DCT. To reveal the cellular localization pattern of phosphorylated claudin-16 along the nephron, we performed colocalization analyses using molecular markers against each nephron segment (Fig. 1). To our surprise, in wildtype (WT) mouse kidneys, phosphorylated claudin-16 proteins were not found in the TAL (counterstained with Tamm–Horsfall protein [THP] [15]), but detected in the luminal membrane of the DCT, including the initial segment of DCT, DCT1 (counterstained with parvalbumin [16]), and the late segment of DCT, DCT2 (counterstained with calbindin-D28K [16]). The CNT/CD, counterstained with aquaporin-2 (AQP2), was without claudin-16 expression. Immunostaining of claudin-16–null mouse kidneys revealed no CLDN16-P signal (*SI Appendix*, Fig. S4). Gesek and Friedman described an immortalized mouse distal convoluted tubule (MDCT) cell line that expresses the thiazide-sensitive Na-Cl cotransporter and the PTH receptor (17). We asked if claudin-16 phosphorylation could be detected in the MDCT cells by an independent biochemical approach. Knowing that the claudin-16 antibody against the carboxyl-terminal domain was not able to recognize the phosphorylated claudin-16 protein, we tagged claudin-16 with the HA polypeptide on its amino terminus (13). To separate phosphorylated claudin-16 from its unphosphorylated form, we performed Phos-tag SDS/PAGE and Western blot on MDCT cell lysates transfected with HA-tagged claudin-16 proteins. Phos-tag is a Mn^{++}-chelating compound that binds specifically to the phosphorylated residues in a protein and retards its migration during SDS/PAGE (18). Phos-tag SDS/PAGE has been used to identify the phosphorylated residue in claudin-2 protein (19). Immunoblotting after Phos-tag SDS/PAGE revealed that HA-tagged WT claudin-16 migrated as 2 major bands, one at its characteristic molecular weight (25 kDa) and the other at a higher molecular weight (30 kDa; *SI Appendix*, Fig. S5). The upper band was sensitive to λ-phosphatase treatment, indicating that it represents the phosphorylated claudin-16. Note that the size of the upper band (30 kDa) is not the true size of phosphorylated claudin-16 protein but only reflects the retarded migration of phosphorylated protein inside the Phos-tag–containing gel. Mutation of claudin-16 at threonine (T) residue 303 to arginine (R) resulted in the loss of the upper phosphorylated band (*SI Appendix*, Fig. S5), suggesting that claudin-16 is phosphorylated at T303 in the MDCT cells.

Phosphorylated Claudin-16 Increases the Membrane Permeability to Ca^{2+} in Trpv5-Expressing Kidney Epithelial Cells. Unlike the TAL, where Ca^{2+} is transported via the paracellular pathway, the DCT handles Ca^{2+} reabsorption via the transcellular channel in the apical membrane and the Ca^{2+}/Na^{+} exchanger or the Ca^{2+} pump in the basolateral membrane. The Trpv5 channel in the apical membrane forms the rate-limiting step of transepithelial Ca^{2+} transport in the DCT (6). To address if phosphorylated claudin-16 can directly regulate Trpv5 channel conductance, we created a phosphomimetic mutation in claudin-16 by substituting glutamic acid (E) for threonine (T) at residue 303 and cotransfected

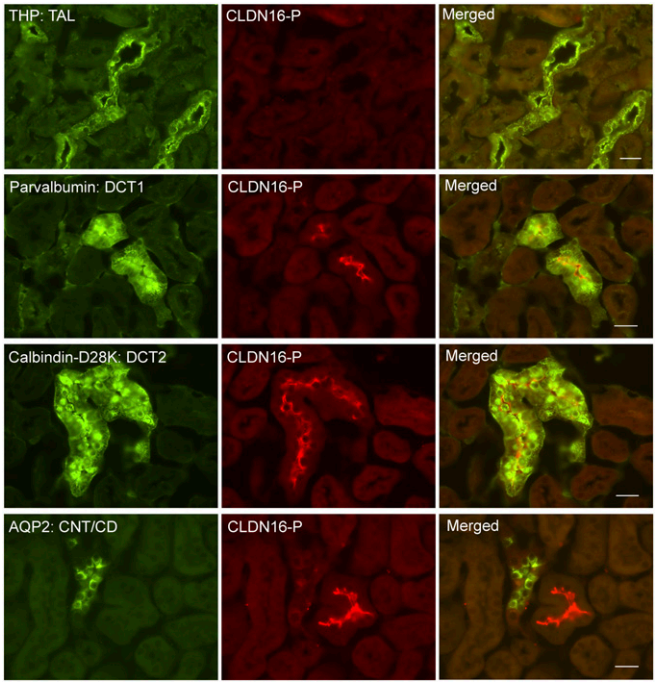

Fig. 1. Phosphorylated claudin-16 protein localization in the kidney. Dual immunofluorescent staining of phosphorylated claudin-16 protein (CLDN16-P) with a TAL marker (THP), with a DCT1 marker (parvalbumin), with a DCT2 marker (calbindin-D28K), and with a CNT/CD marker (AQP2). (Scale bar: 20 μm.)

the mutant claudin-16 with Trpv5 into the HEK293 cells. WT claudin-16 and a mutant claudin-16, which harbors the T303R substitution discovered from a cohort of FHHNC patients, were analyzed in parallel. Notably, T303R is a dephosphorylated mutation. To directly measure the membrane permeability to Ca^{2+}, we performed in vitro [45]Ca^{2+} uptake assays in doubly transfected HEK293 cells (*Methods*). Because Trpv5 is rapidly inactivated by intracellular Ca^{2+} (20), we pretreated the cells with a cell-permeable Ca^{2+} quenching reagent, BAPTA-AM (*Methods*). We then used an extracellular condition of 0.1 mM Ca^{2+} containing 1 μCi/mL [45]Ca^{2+} to elicit Ca^{2+} influxes as described before by a published protocol (21). The Ca^{2+} influx rate, reflected by the intracellular [45]Ca^{2+} level, showed no significant change in cells transfected with claudin-16 or its mutants alone, indicating that claudin-16 does not make a Ca^{2+} channel by itself (Fig. 2). Transfection of Trpv5 alone elicited a 3.8-fold increase in [45]Ca^{2+} influx rates ($P < 0.01$; $n = 5$ transfections). Cotransfection of Trpv5 with claudin-16 (T303E) further increased the [45]Ca^{2+} influx rates, which were now 2.3-fold higher than the levels in Trpv5 transfection alone ($P < 0.01$; $n = 5$ transfections; Fig. 2). By contrast, WT claudin-16 or its dephosphorylated form, T303R, was not able to regulate Trpv5's function (Fig. 2).

Phosphorylated Claudin-16 Increases Trpv5 Current Density in Kidney Epithelial Cells. Knowing that the [45]Ca^{2+} intake assay reflects the accumulative nature of membrane Ca^{2+} permeation over time, we next adopted the patch-clamp technique to capture transient Trpv5 current changes in the presence of claudin-16 proteins. Because extracellular Ca^{2+} rapidly inhibits Trpv5 conductivity (22, 23), we used Na^+ as the charge carrier to record Trpv5 channel current under whole-cell patch-clamp configuration (24, 25). The HEK293 cells were used as a research model because there was no endogenous Trpv5 current in these cells (21, 25). As previously reported (26), virtually no channel current was observed at positive membrane potentials in Trpv5-expressing HEK293 cells (Fig. 3*A*). The current-voltage (I-V) curve established in response to a voltage ramp from −150 mV to −50 mV revealed a linear relationship and reflected the Trpv5 channel conductance (Fig. 3*A*). It was clear from the I-V curve that the phosphomimetic mutant T303E, but not the wildtype claudin-16 or the dephosphorylated mutant T303R, increased the Trpv5 channel conductance. We then measured the current densities for Trpv5 at −150 mV by normalizing current amplitude to cell capacitance. We found that the T303E mutant, but not the wildtype claudin-16 or the T303R mutant, consistently stimulated the Trpv5 conductivity and significantly increased its current density in doubly transfected cells compared with control cells that expressed Trpv5 with an empty vector ($P < 0.0001$; $n \geq 5$ recordings), or cotransfected cells that expressed Trpv5 with wildtype claudin-16 ($P < 0.05$; $n \geq 5$ recordings) or with T303R mutant claudin-16 ($P < 0.0001$; $n \geq 5$ recordings; Fig. 3*B*). Note that the wildtype claudin-16 group, but not the T303R mutant group, showed a large variation in Trpv5 current density, which might be caused by endogenous kinase activity randomly phosphorylating claudin-16.

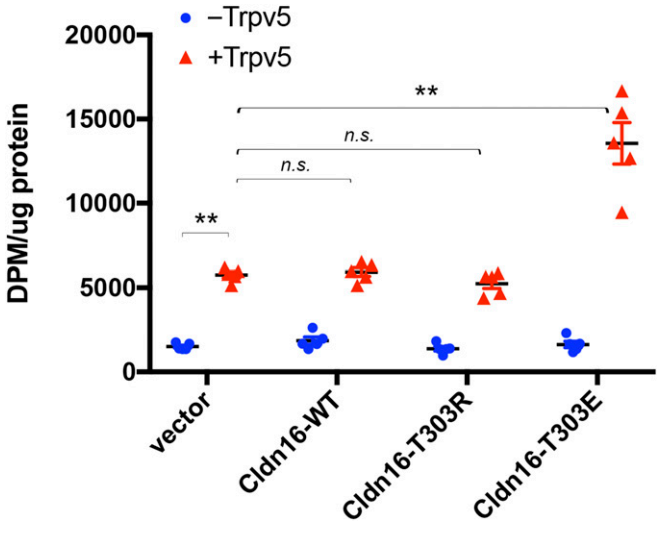

Fig. 2. Effects of claudin-16 phosphorylation on membrane Ca^{2+} permeability in the presence or absence of Trpv5. Shown in the statistical graph are assays of [45]Ca^{2+} influx rates in cells expressing Trpv5 with various claudin-16 proteins, including wildtype (WT) and dephosphorylated (T303R) and phosphomimetic (T303E) claudin-16 (**$P < 0.01$; $n = 5$ transfections). n.s., not significant.

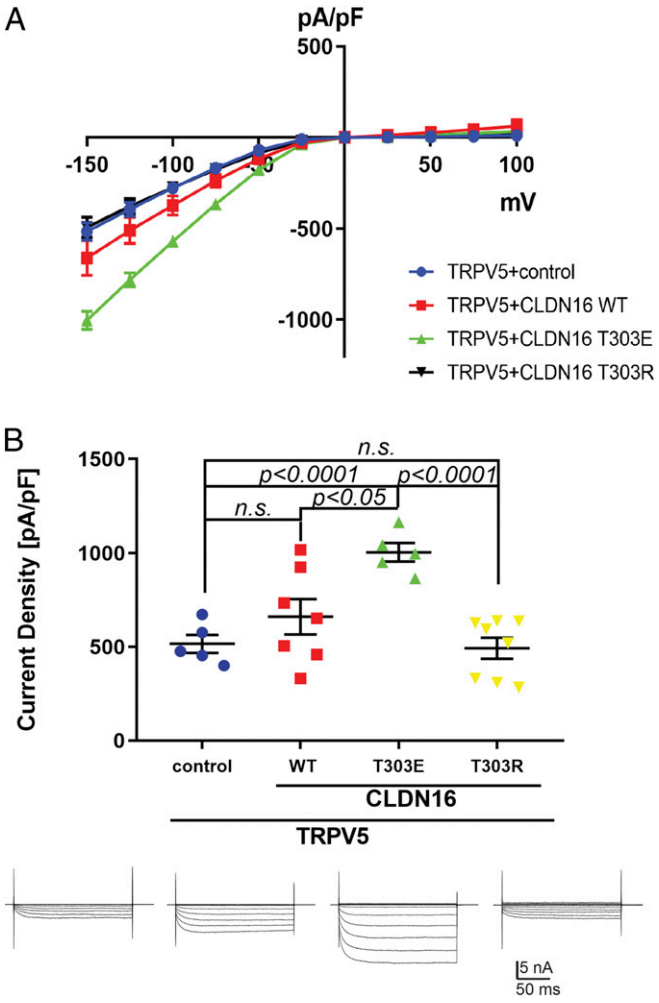

Fig. 3. Claudin-16 mutant T303E increases Trpv5 current density. (*A*) The steady-state current-voltage (I-V) curve revealed a characteristic inwardly rectifying Trpv5 currents in HEK293 cells transfected with Trpv5 plus empty vector versus claudin-16 WT, T303E, or T303R mutant ($n \geq 5$ recordings for each group). Trpv5 current density (current normalized to cell plasma membrane area, pA/pF; mean ± SEM) was evoked by test pulses from −150 to +100 mV, with +25-mV increments, for 200 ms. (*B*) In HEK293 cells coexpressing Trpv5 with claudin-16 variants, T303E but not WT or T303R claudin-16 increased TRPV5 current density compared with control (Trpv5+empty vector; $P < 0.0001$; $n \geq 5$ recordings). Representative current traces are shown below each study group. n.s., not significant.

Phosphorylated Claudin-16 Increases Trpv5 Membrane Abundance in Kidney Epithelial Cells. The conductance of an ion channel is determined by its single-channel conductivity (G), its open

probability (P_o), and its membrane abundance (N). To address if claudin-16 affected Trpv5 cell surface abundance, we measured the cell-surface biotinylated Trpv5 levels with the membrane-impermeable Sulfo-NHS-SS-biotin labeling technique described before (27). In HEK293 cells, transfection of phosphomimetic claudin-16 (T303E) increased the cell surface abundance levels of Trpv5 (glycosylated form, 92 kDa; and core protein, 82 kDa) by 1.95-fold and 4.90-fold, respectively ($P < 0.05$; $n = 3$ transfections), while dephosphorylated claudin-16 (T303R) slightly but significantly decreased the cell surface abundance levels of core Trpv5 protein ($P < 0.05$; $n = 3$ transfections), compared with control transfection (Fig. 4). Wildtype claudin-16 showed no significant effect in this assay. The total cellular abundance levels of Trpv5 were not changed by WT or claudin-16 variants (*SI Appendix*, Fig. S6). Although we know claudin-16 does not form a membrane channel on its own, it may still alter the structure of Trpv5 via molecular interactions. The T303R mutation could be more than a simple null mutation. Therefore, further single-channel recordings will be needed to determine if claudin-16 regulates the G or P_o of Trpv5.

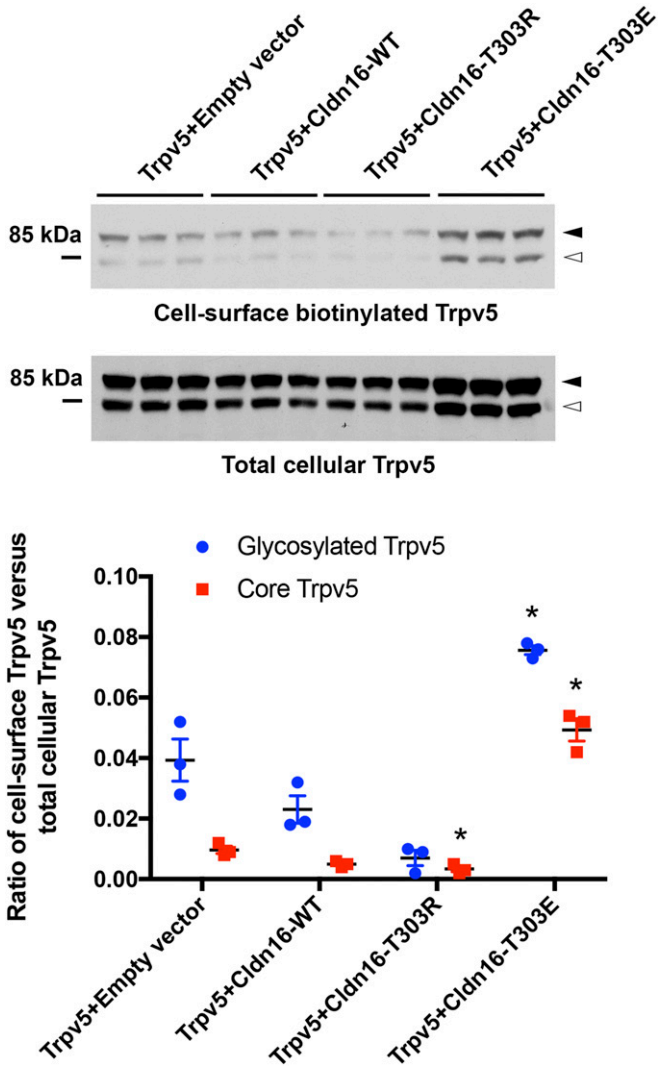

Fig. 4. Claudin-16 mutant T303E increases Trpv5 membrane abundance levels. Cell-surface biotinylation assays of Trpv5 abundance levels in cells expressing Trpv5 with claudin-16 variant proteins, including wildtype (WT) and dephosphorylated (T303R) and phosphomimetic (T303E) claudin-16. Trpv5 proteins migrate as 2 separate bands on PAGE gel: 82-kDa core protein (white arrowhead) and 92-kDa glycosylated protein (black arrowhead; $*P < 0.05$; $n = 3$ transfections versus empty vector).

Reduced Luminal Membrane Trpv5 Abundance in Claudin-16 Knockdown Mouse DCT Tubules. Because endogenous Trpv5 currents have never been captured in vivo in the DCT tubules, we sought evidence that claudin-16 may regulate Trpv5 membrane abundance in the mouse kidney. To address if the membrane abundance of Trpv5 in the DCT is regulated by claudin-16, we adapted a biochemical protocol to extract the luminal membrane from freshly isolated mouse distal tubules according to a published study (28) (*Methods*). Claudin-16 knockdown (KD) mice have been generated, described, and validated by us before (5). The KD mice developed profound hypercalciuria previously attributed to the loss of claudin-16 function in the TAL (5, 29). The luminal membranes from WT or KD mouse distal tubules ($n = 5$ animals) were pooled and immunoblotted to quantify Trpv5 protein levels. On the densitometric scale, the luminal membrane abundances of glycosylated Trpv5 (92 kDa) and core Trpv5 (82 kDa) were reduced by ~70% and ~95%, respectively, in KD mouse kidneys compared with WT mouse kidneys (Fig. 5*A*). The NCC protein abundance was measured and used as a loading control for the membrane preparation. The Trpv5 mRNA levels in the kidney were not different between WT and KD animals (Fig. 5*B*). To show if Trpv5 localization is affected by the ablation of claudin-16, we performed immunohistological analyses on rapidly frozen, freshly cut kidney sections from WT and KD mice. In WT mouse kidney sections, the Trpv5 proteins were clearly seen on the luminal membrane of the DCT2 tubules, which were counterstained with calbindin-D28K (Fig. 5*B*). In contrast, the luminal membrane localization of Trpv5 was nearly completely abolished in the KD mouse DCT2 tubules (Fig. 5*B*). Only remnant signals can be found intracellularly in these tubules. An independent Trpv5 antibody was used to confirm the effects of claudin-16 deletion on Trpv5 localization in the DCT2 tubules (*SI Appendix*, Fig. S7). Low-magnification images of immunolabeled Trpv5 in the DCT2 tubules from WT and KD mouse kidneys are shown in *SI Appendix*, Fig. S8. We then asked if deletion of claudin-16 may cause compensatory changes in Trpv5 localization in the DCT1 or in the CNT. The expression of Trpv5 was very low in the DCT1 tubules (counterstained with parvalbumin) from the WT mouse kidney, consistent with a previous report (30). No compensatory change was found in the claudin-16 KD mouse DCT1 tubules (*SI Appendix*, Fig. S9). The Trpv5 localization was mainly cytoplasmic in the CNT tubules (counterstained with Aqp2) from the WT mouse kidney, consistent with previous observation (30). No change in Trpv5 localization was found in claudin-16 KD mouse CNT tubules (*SI Appendix*, Fig. S10). Notably, the reduced membrane abundance of Trpv5 in claudin-16 KD mouse DCT2 tubules could be attributed to a direct regulatory requirement of claudin-16 for Trpv5 membrane localization and stability, or to a secondary effect of hypercalciuria caused by claudin-16 dysfunction in the TAL tubules. Further analyses of tubule-specific claudin-16 knockout mouse models will be needed to resolve the in vivo role of claudin-16 in Trpv5 regulation.

Protein Interaction between Trpv5 and Phosphorylated Claudin-16. Knowing that claudin-16 can alter Trpv5 membrane abundance and channel conductance, we reasoned that these 2 proteins may directly interact. To determine the interaction between claudin-16 and Trpv5 in yeast cell membrane, we used the split-ubiquitin yeast 2-hybrid (Y2H) membrane protein interaction assay in *Saccharomyces cerevisiae* as described by us before (31). In the Y2H assay, a membrane protein of interest, the "bait," is fused to the C-terminal half of ubiquitin (Cub) along with an artificial transcriptional factor (TF). The putative interacting membrane protein, called the "prey," is fused to the N-terminal half of ubiquitin (Nub). Upon interaction of the 2 proteins, the

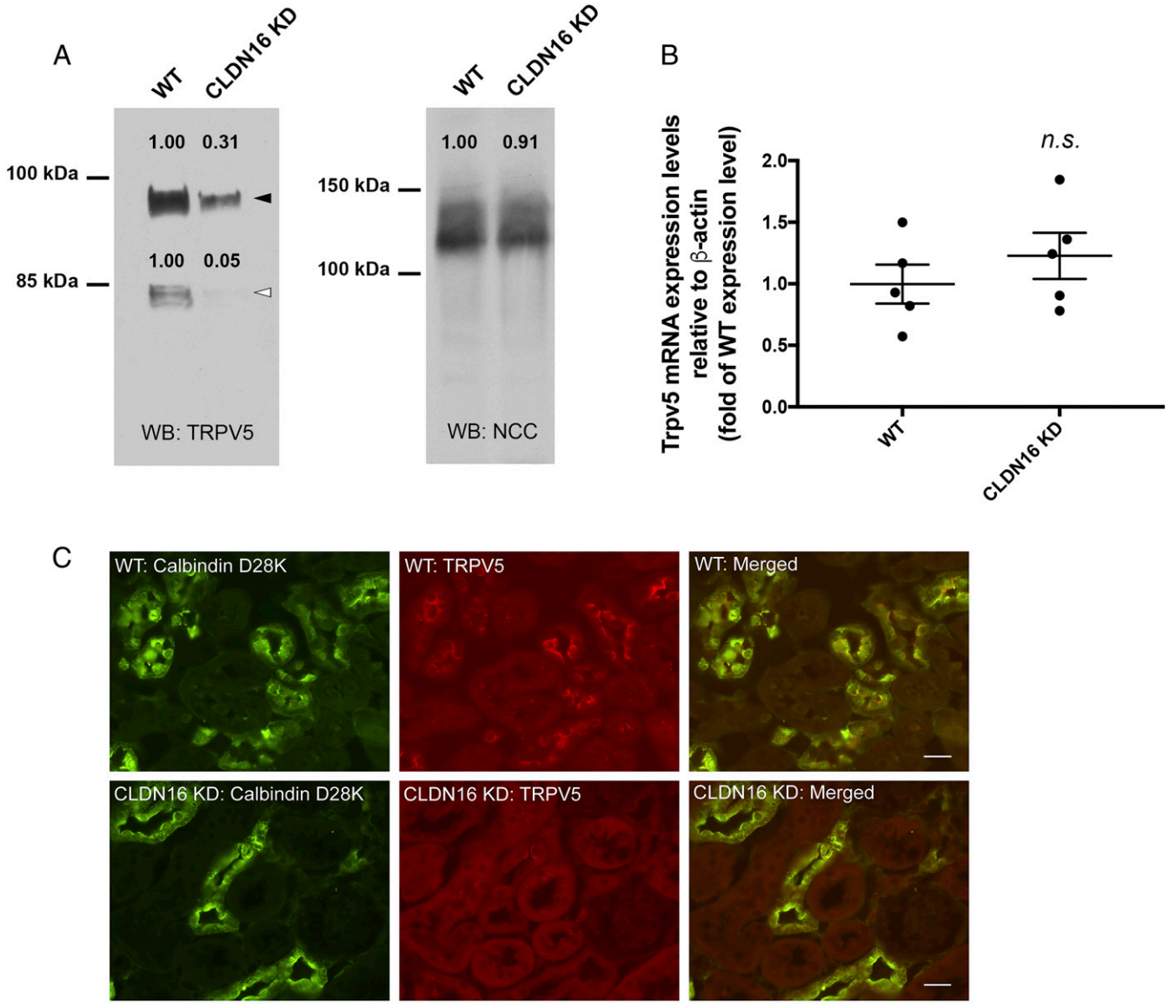

Fig. 5. Trpv5 protein abundance and localization in claudin-16 KD mouse kidney. (*A*) Luminal membranes from mouse distal tubular cells were extracted, pooled, and assayed for Trpv5 protein abundance levels. Trpv5 proteins migrate as 2 separate bands on PAGE gel: 82-kDa core protein (white arrowhead) and 92-kDa glycosylated protein (black arrowhead). NCC proteins were used as loading control. (*B*) Whole-kidney Trpv5 mRNA levels were measured with real-time PCR (n.s., not significant; $n = 5$ animals). (*C*) Dual immunofluorescent staining of Trpv5 with the DCT2 marker (calbindin-D28K) on the kidney sections from WT and claudin-16 KD mice. The rabbit anti-Trpv5 from Alpha Diagnostics was used in this experiment. (Scale bar: 20 μm.)

reconstitution of ubiquitin (Cub+Nub) occurs. Ubiquitin is then recognized by ubiquitin-specific proteases, resulting in the cleavage of the TF. The released TF then enters the nucleus and activates transcription of the reporter genes *HIS3* and *lacZ*. Our data show that WT and variant claudin-16 (T303E and T303R) all interact with Trpv5 in the yeast NMY51 strain (Fig. 6*A*). The levels of interaction of Trpv5 with various claudin-16 isoforms were similar as determined by quantitative β-gal assay, suggesting that the interaction is likely mediated by the transmembrane domains in claudin-16 (Fig. 6*A*). To document claudin-16 and Trpv5 interaction in mammalian cell membrane, we performed coimmunoprecipitation of phosphomimetic claudin-16 (T303E) and Trpv5 from the plasma membrane of transfected HEK293 cells. Because our claudin-16 antibody was raised against the carboxyl-terminus of claudin-16 protein, where phosphorylation may occur to alter the binding affinity of the antibody, we fused a GFP protein to the amino terminus of claudin-16 and immunoprecipitated the claudin-16 proteins with an anti-GFP antibody. To ensure Trpv5 can be effectively pulled down, we tagged the FLAG sequence to Trpv5 and immunoprecipitated the fusion proteins with an anti-FLAG antibody. Immunoblots showed that anti-GFP antibody coprecipitated Trpv5 in HEK293 cells expressing phosphomimetic claudin-16 (T303E; Fig. 6 *B*, *Left*), whereas anti-FLAG antibody reciprocally precipitated claudin-16 (Fig. 6 *B*, *Right*). To test whether claudin-16 was colocalized with Trpv5, we analyzed the subcellular localization of phosphorylated claudin-16 and Trpv5 in the mouse kidney. In WT mouse kidney distal tubules, phosphorylated claudin-16 proteins (stained with anti–CLDN16-P antibody) were colocalized with Trpv5 proteins in the luminal membrane (*SI Appendix*, Fig. S11).

Phosphorylation Delocalizing Claudin-16 from Tight Junction. To ask why phosphorylated claudin-16 was targeted to the luminal

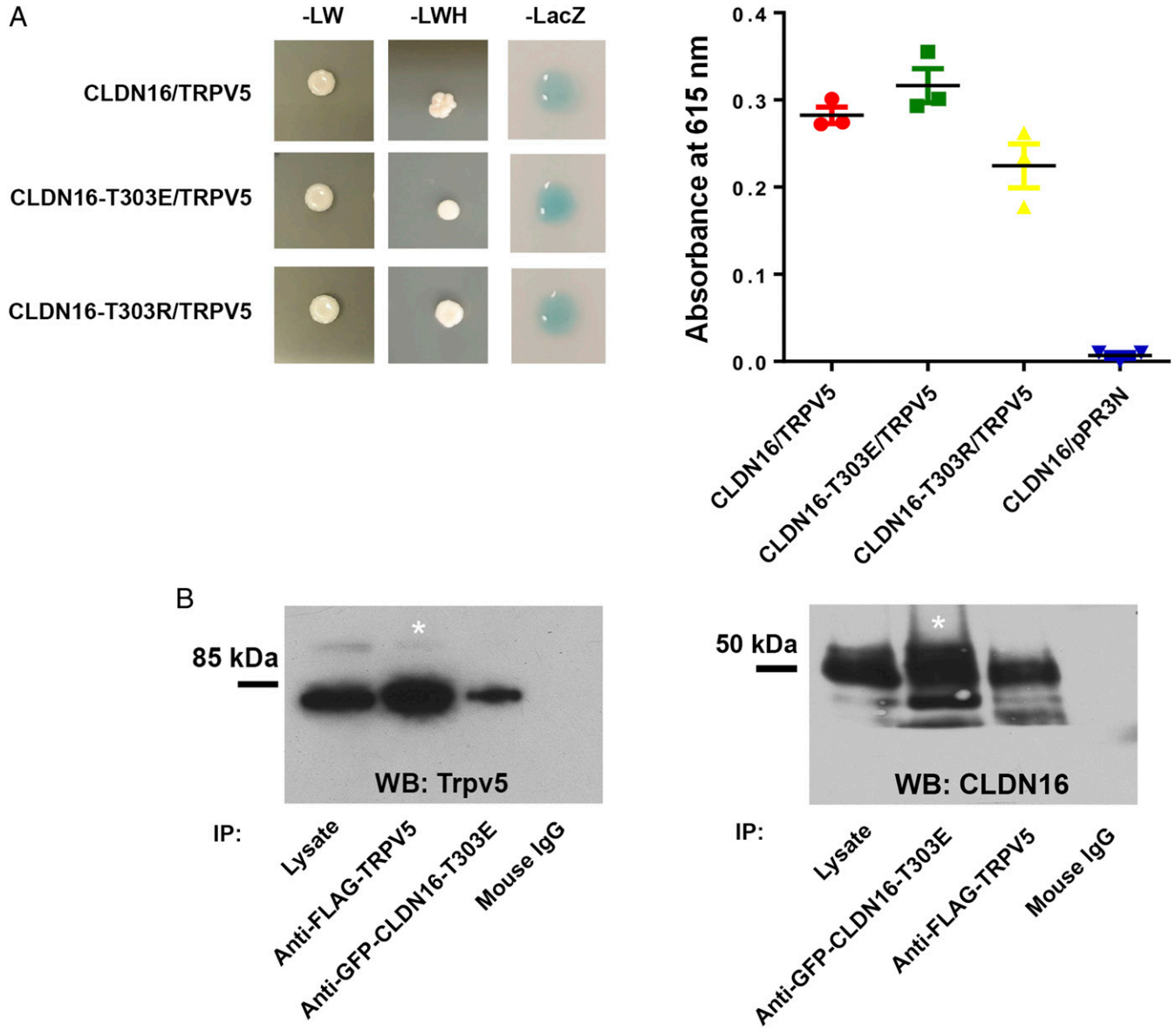

Fig. 6. Protein interaction of claudin-16 with Trpv5. (*A*) Y2H assays showing interaction of Trpv5 with CLDN16-WT, CLDN16-T303E, and CLDN16-T303R. Shown are plates with selective medium lacking leucine and tryptophan (–LW), indicating the transforming of both bait and prey vectors; with SD-LWH, indicating the expression of reporter gene *HIS3*; and β-galactosidase assay (A615 values) for quantification of interaction strength ($n = 3$ clones). Negative control is measured as interaction of CLDN16 bait vector with an empty prey vector (pPR3N). (*B*) Coimmunoprecipitation assay showing Trpv5 (Flag-Trpv5) interacts with phosphomimetic claudin-16 (GFP-Cldn16-T303E) in transfected HEK293 cells. Asterisk indicates that lane shows 10% of input amount as in other lanes.

membrane instead of the TJ in the DCT tubules (Fig. 1), we reckoned that phosphorylation may have weakened the interaction between the carboxyl-terminal PDZ-binding motif (-TRV) in claudin-16 and the TJ peripheral protein ZO-1. To test this hypothesis, we first addressed if phosphorylation alone was sufficient to alter the subcellular localization of claudin-16 in polarized renal epithelial cells. We previously described an epithelial cell model, the LLC-PK1 cell, to study the paracellular permeabilities of claudin-16 (31). When the LLC-PK1 cells were seeded onto Transwell to allow polarization and establishment of the TJs, WT claudin-16 proteins were found exclusively in the TJ and colocalizing with ZO-1 (Fig. 7 *A*, *Top*). Phosphomimetic claudin-16 proteins (T303E), however, were largely delocalized from the TJ but relocated to the apical membrane (Fig. 7 *A*, *Bottom*; *SI Appendix*, Fig. S12 shows a side view from 3D-rendered *Z*-stacks). We then investigated if phosphorylation disrupted the interaction between claudin-16 and ZO-1. To address this possibility, we cotransfected GFP-fused claudin-16 and Myc-tagged ZO-1 into HEK293 cells and performed coimmunoprecipitation with anti-GFP and anti-Myc antibodies. Immunoblots showed that WT claudin-16 (Fig. 7 *B*, *Left*), but not phosphomimetic claudin-16 (T303E; Fig. 7 *B*, *Right*), pulled down ZO-1 from the plasma membrane of HEK293 cells.

PTH Regulation of Claudin-16 Phosphorylation. Finally, we addressed the physiological role of claudin-16 phosphorylation in the kidney. Knowing that phosphorylated claudin-16 facilitated Ca^{2+} permeation through the Trpv5 channel in the DCT, we hypothesized the phosphorylation level in claudin-16 might be regulated by extracellular Ca^{2+} levels as a part of systemic Ca^{2+} homeostasis.

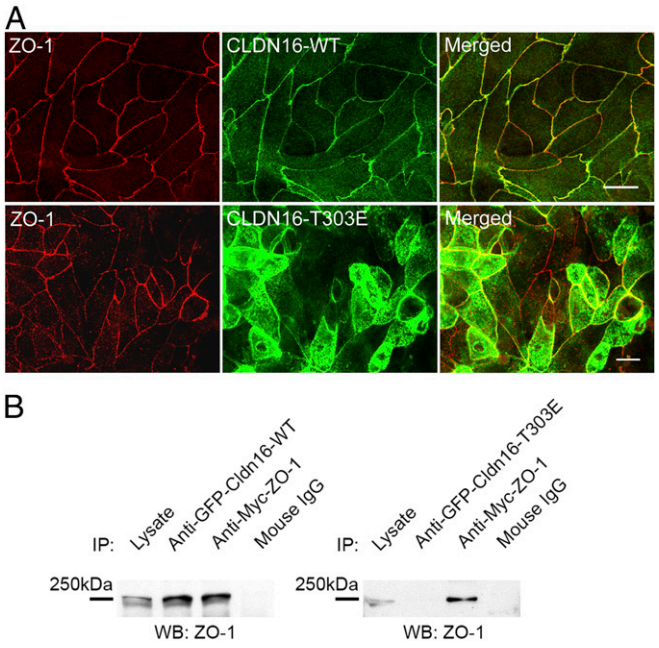

Fig. 7. TJ localization and ZO-1 interaction of phosphorylated claudin-16. (*A*) Confocal microscopy showing TJ localization of wildtype claudin-16 and apical membrane localization of phosphomimetic claudin-16 in transfected LLC-PK1 cells. The TJ was labeled with an antibody against ZO-1. (Scale bar: 10 μm.) (*B*) Coimmunoprecipitation assay showing that wildtype claudin-16 (GFP-Cldn16-WT) but not phosphomimetic claudin-16 (GFP-Cldn16-T303E) interacts with ZO-1 (Myc-ZO-1) in transfected HEK293 cells.

To induce an extracellular Ca^{2+} excess, we treated animals, age-matched (8 wk) and sex-matched (male) mice, with high-Ca^{2+} diet (5% Ca^{2+}) versus basal diet (0.6% Ca^{2+}) for 6 consecutive days. High-Ca^{2+} diet induced higher plasma Ca^{2+} levels in experimental mice (*SI Appendix*, Fig. S13*A*). Distal tubules were isolated from these animals at the end of treatment by a protocol described elsewhere in this study and were probed for changes in claudin-16 phosphorylation levels. Immunoblots with anti–CLDN16-P antibody showed an 87% decrease ($P < 0.01$; $n = 4$ animals) in phosphorylated claudin-16 protein levels from high-Ca^{2+} diet-treated mice compared with mice maintained on basal diet (*SI Appendix*, Fig. S13*B*). Immunostaining of mouse kidney sections revealed a dramatic decrease in the luminal membrane abundance levels of phosphorylated claudin-16 in the DCT tubules (counterstained with parvalbumin and calbindin-D28K) from high-Ca^{2+} diet-treated animals (*SI Appendix*, Fig. S13*C*). High extracellular Ca^{2+} levels may signal through the Ca^{2+} sensing receptor (CaSR), calcitriol [$1,25(OH)_2D_3$] and the parathyroid hormone (PTH). Among them, PTH is best known for increasing the membrane abundance and the open probability of Trpv5 channel in the DCT tubules (21, 32). We then asked if claudin-16 phosphorylation was under direct control by PTH. PTH binds to and activates the PTH/PTHrP receptor (PTH1R), a G protein-coupled receptor that is expressed in many tissues but has the highest expression in the kidney (33). To selectively delete PTH1R in the distal tubules, we crossed the $PTH1R^{fl/fl}$ mice to the Ksp-Cre mice as described before (34). In freshly isolated distal tubules from the Ksp-Cre/$PTH1R^{fl/fl}$ (PTH1R KO) mice (9 wk old, mixed sex), the phosphorylated claudin-16 protein levels were reduced by 91% ($P < 0.01$; $n = 3$ animals) compared with the levels in the $PTH1R^{fl/fl}$ (9-wk-old littermate control) mice (Fig. 8*A*). In kidney sections of the PTH1R KO mice, the phosphorylated claudin-16 proteins nearly completely disappeared from the luminal membrane in the DCT tubules (counterstained with parvalbumin and calbindin-D28K; Fig. 8*B*). Only remnant signals were seen intracellularly in these tubules.

Discussion

Our prior work has established that claudin-16 and claudin-19 form a heteromeric paracellular cation channel in the TAL of the kidney, which 1) permeates Ca^{2+} and Mg^{2+} and 2) generates a lumen-positive diffusion potential that provides the driving force for Ca^{2+} and Mg^{2+} reabsorption (31, 35). Various FHHNC mutations in claudin-16 or claudin-19 were demonstrated to impair the permeating function of the paracellular channel made of claudin-16 and claudin-19 (13, 31, 36), allowing us to attribute FHHNC to dysfunction in the TAL of the kidney. However, this theory needs significant revision in the light of new results. Simon et al. made the first observation that the mRNA of claudin-16 was expressed by the DCT, although the protein of claudin-16 can only be found in the TAL (2). Our finding that the claudin-16 protein is expressed by the DCT, albeit taking a phosphorylated form to evade detection by regular antibodies, would indicate that the pathogenesis of FHHNC involves the molecular pathways in the DCT. Among the claudin-16 mutations that cosegregate with FHHNC, the majority are loss-of-function mutations, including premature termination, splice site alteration, frame shift, and amino acid substitution causing protein structural alterations (2, 10, 36, 37). These mutations would simultaneously shut off the transport pathways in the TAL and the DCT, causing the devastating phenotypes of FHHNC. The c.908C>G (p.T303R) mutation is unique. Patients carrying this mutation showed severe hypercalciuria but little disturbance in renal Mg^{2+} excretion (11). The mild phenotype regarding Mg^{2+} metabolism in these patients would suggest the T303R mutation reduces the paracellular conductance in the TAL to a small extent. We now know that the T303R mutation is unable to facilitate transcellular Ca^{2+} permeation via Trpv5 in kidney cells. From a pathogenic point of view, the phenotype due to T303R mutation might be considered as a hypercalciuric state escaping the physiologic regulation of renal Ca^{2+} reabsorption. The PTH–to–claudin-16 phosphorylation pathway could serve as a key mechanism to defend renal Ca^{2+} loss. Because the PTH–to–claudin-16 pathway regulates the membrane abundance of Trpv5 channel, it may synergize with the PTH-to-PKA pathway to augment Ca^{2+} reabsorption in the DCT, the latter being shown to increase the open probability of Trpv5 channel (21). Other signaling pathways may also play roles in claudin-16 phosphorylation, such as CaSR, calcitriol, Klotho, and WNKs. In particular, WNK4 has been shown to phosphorylate claudins as its selective substrates in several model systems (38, 39). The transgenic mice carrying a gain-of-function mutation in WNK4 developed pronounced hypercalciuria (16). Finally, since claudin-19 is expressed in the DCT (40), it may also play a role in membrane Ca^{2+} permeability via interaction with claudin-16.

Claudin phosphorylation may separate its function in transcellular pathway from paracellular pathway. Our results indicate that phosphorylation dynamically shuffles the claudin-16 proteins between the TJ and the apical membrane. Unphosphorylated claudin-16 proteins travel to the TJ, where they function as paracellular channels, while phosphorylated claudin-16 proteins preferably accumulate in the apical membrane, where they could interact with transcellular ion channels. Ikari and colleagues have revealed an additional phosphorylation site in claudin-16 at its carboxyl terminus (S287 in human claudin-16; S217 in mouse claudin-16) (41). Phosphorylation at this site is essential for claudin-16's interaction with ZO-1 and localization to the TJ. In general, phosphorylation appears to partition the claudin proteins into different membrane compartments. For example, phosphorylation of claudin-2 at the site S208 promotes its plasma membrane retention by altering its lipid binding propensity (19). Prior evidence supports the theory that claudins can regulate the

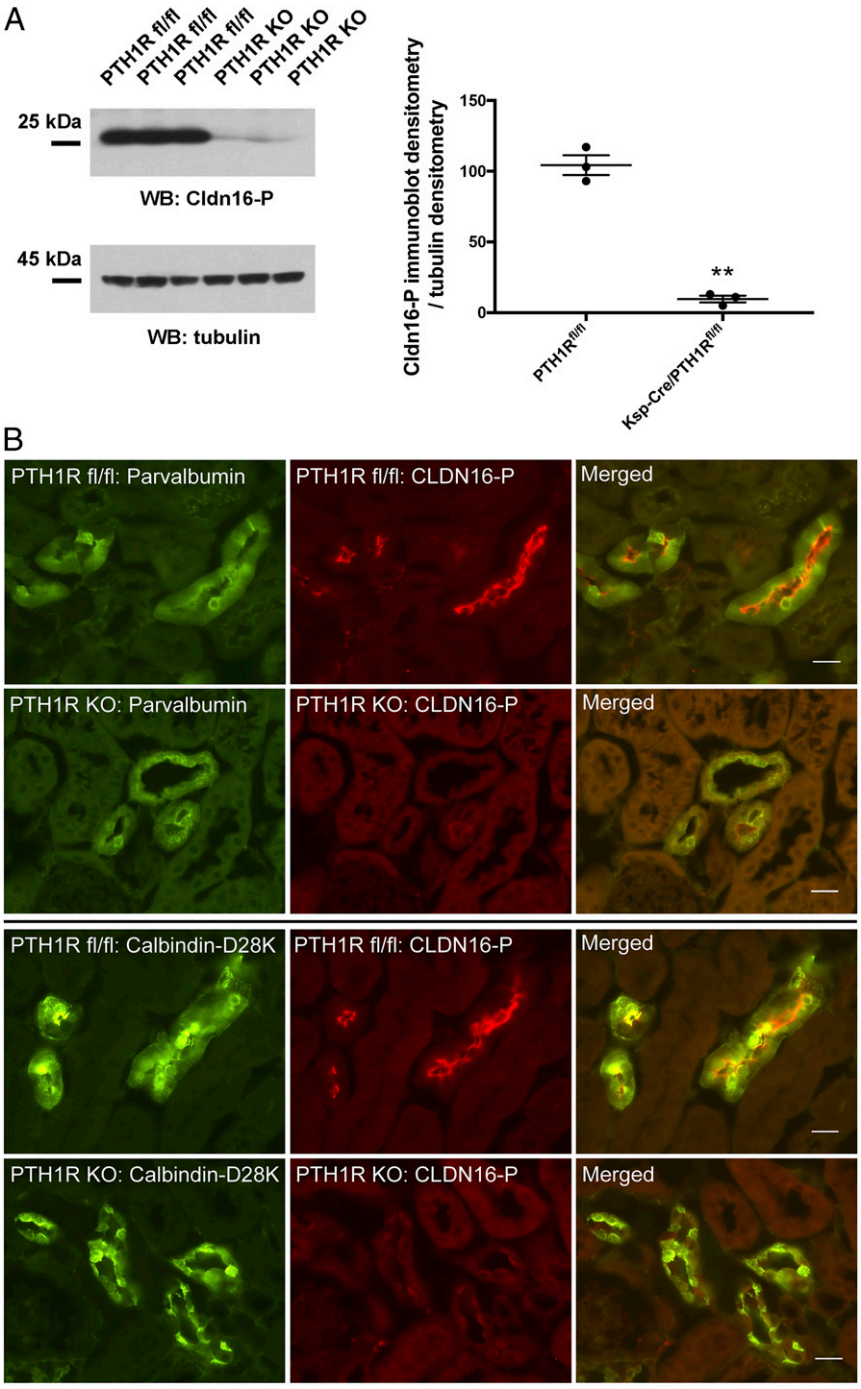

Fig. 8. Claudin-16 phosphorylation levels in PTH1R KO mice. (*A*) Freshly isolated mouse distal tubular cells from Ksp-Cre/PTH1R$^{fl/fl}$ mice were lysed in Laemmli buffer and immunoblotted against anti-CLDN16-P antibody to reveal claudin-16 phosphorylation levels. Anti-tubulin antibody was used for loading control (**$P < 0.01$; $n = 3$ animals). (*B*) Dual immunofluorescent staining of phosphorylated claudin-16 protein (CLDN16-P) with the DCT markers (parvalbumin and calbindin-D28K). (Scale bar: 20 μm.)

transcellular pathway. For example, claudin-16 has been shown to increase transcellular Cl^- permeability in the MDCK cells via interaction with the calcium-activated chloride channel (42). Therefore, it is not surprising to find that claudin-16 regulates Trpv5 conductance or even acts as a regulatory accessory to the channel. Whether claudin-16 interacts with other Ca^{2+} or Mg^{2+} channels will be an intriguing point to follow. Notably, phosphorylated claudin-16 proteins are expressed by the DCT1 tubules, where Trpv5 proteins are maintained at low levels. Yu and colleagues made a seminal discovery that voltage-gated calcium channels were abundantly expressed by the DCT (43). Phylogenetic analyses have suggested that claudins and voltage-gated calcium channel γ subunits (CACNG) share a common ancestral root (44). Both classes of proteins carry the same characteristic motif (-GLWCC; PROSITE ID PS01346) in the first extracellular loop domain (45). If claudins truly behave like a γ subunit to the channel, exciting new biologies will unfold with regard to claudins in organ functions not limited to the kidney.

Materials and Methods

Reagents, Antibodies, Cell Lines, and Animals. The following antibodies were used: anti-GFP (IP grade; Abcam), anti-Myc (Roche), anti-Flag (IP grade; Sigma), anti–claudin-16 (35), anti-NCC (Santa Cruz Biotech), anti-NCC (Millipore), anti-Aqp2 (Santa Cruz Biotech), anti-parvalbumin (Swant), anti-calbindin-D28K (Swant), anti-THP (R&D Systems), anti-tubulin (University of Iowa Hybridoma Bank), anti-Trpv5 (Abcam) (46), and anti-Trpv5 (Alpha Diagnostics) (47). Anti–CLDN16-P antibody was made against the phosphorylated peptide AKMYAVD(pT)RV. The antiserum was purified by affinity chromatography and cross-absorbed against the unphosphorylated peptide AKMYAVDTRV. The peptide sequence used to generate the anti–CLDN16-P antibody is conserved between human and mouse claudin-16. HEK293 cells (ATCC) and MDCT cells (ATCC) were cultured in Dulbecco's modified Eagle's medium (DMEM) supplemented with 10% FBS, penicillin/streptomycin, and 1 mM sodium pyruvate. All mice were bred and maintained according to the Washington University animal research requirements, and all procedures were approved by the Washington University institutional animal research and care committee under the license No. 20170051. The claudin-16 knockdown mice were described before (5). The Ksp-Cre/Pth1r$^{fl/fl}$ mice were described before (34). All animals had free access to water and were housed in a 12-h light cycle. Blood samples were taken by cardiac puncture rapidly after initiation of terminal anesthesia and centrifuged at 4 °C for 10 min. Kidneys were dissected out and immediately frozen at −80 °C.

Molecular Cloning, Transfection, and Retrovirus Production. The following full-length genes were cloned into various mammalian expression vectors: human claudin-16 (GenBank accession no. AF152101) to pEGFP-C1 vector (Clontech), human Trpv5 (GenBank accession no. NM_019841) to pcDNA3.1 vector (Invitrogen) or pCMV-Flag vector (Clontech), and human ZO-1 (GenBank accession no. NM_003257) into pCB-Myc vector (Addgene). The site-directed mutagenesis was performed on claudin-16 to generate T303R and T303E mutations with a PCR-based mutagenesis method (Stratagene). Molecular clones for each of the mutants were verified by DNA sequencing. HEK293 cells were transfected with these vectors individually or in combination by using Lipofectamine 3000 (Invitrogen). VSV-G pseudotyped retroviruses were produced in HEK293 cells and used to infect LLC-PK1 cells at a titer of 1×10^6 CFU/mL as described previously (13).

Microdissection of Renal Tubules from Mouse Kidney. Mice were anesthetized by isoflurane and by i.p. injections of ketamine and xylazine. The kidney was perfused through the renal artery with 1 mL Ringer's solution containing 1 mg/mL collagenase type II. After perfusion, the kidney was decapsulated and cut into 0.2- to 0.3-mm-thick slices. The kidney slices were gently shaken at 850 rpm to release renal tubules. The tubules were pipetted into a dissection dish containing Ringer's buffer. Each individual tubular segment was cut and sorted using a pair of fine forceps (Dumont no. 5). Approximately 200 sorted tubules from each nephron segment were rapidly frozen in liquid nitrogen.

Real-Time PCR Analysis of mRNA Expression. Total RNA was extracted by using TRIzol (Invitrogen). Cellular mRNA was reverse-transcribed using the SuperScript-III kit (Invitrogen), followed by real-time PCR amplification using SYBR Green PCR Master Mix (Bio-Rad) with the primer pairs as follows: CLDN16, CGAACCTGCGATGAGTACGA and CCAAGGAGCAGGGTGATGAA; Trpv5, GTTCCGAGATGCCAACCGTA and CAAAGTAGCGAGAGGCACCA; NKCC2, GACAACGAGTGTGAGGAGGG and TGATTGAACTCCCCGACGTG; NCC, AGGTCTCACCCTCCTCATCC and GTCGGGAAGGACGTGAACTT; and β-actin, CGTTGACATCCGTAAAGAC and TGGAAGGTGGACAGTGAG. Results were expressed as $2^{-\Delta Ct}$ values with $\Delta Ct = Ct_{gene} - Ct_{\beta\text{-actin}}$.

Isolation of Distal Tubules from Mouse Kidney and Protein Expression Assay. Distal tubules were isolated from the cortices of mouse kidneys by a method modified from Doctor et al. (14). Mice were killed by i.p. injection of an overdose of ketamine. The kidney cortices were removed and minced into 1-mm^3 pieces in DMEM supplemented with 10 mM Hepes and 2 mg/mL Collagenase-I (Worthington Biochemicals). After incubation at 37 °C for 20 min, the tissues were triturated with 13G, 15G, and 17G cannulas sequentially to break the renal tubules into small fragments. The tubular suspension, derived from both proximal tubules and distal tubules, was further separated by centrifugation at 50,000 × *g* at 4 °C in a Percoll gradient solution made of 25%, 35%, 45%, and 55% Percoll in DMEM supplemented with 10 mM Hepes. The distal tubular suspension, recovered from a band in 55% Percoll solution, was washed twice with 1× PBS at 250 × *g* at 4 °C and plated onto culture dishes to examine cell viability. Cell preparation with >90% viability was assayed for protein expression. Approximately 3 to 5 mg (pellet weight) of distal tubules can be obtained from the kidneys of 1 animal. Two biochemical protocols were used to extract the proteins from the distal tubular cell pellets. The total cell lysate was obtained by dissolving the distal tubular cell pellet in Laemmli 2× buffer. The membrane proteins were extracted by dissolving the distal tubular cell pellet in CSK buffer (150 mM NaCl, 1% Triton X-100, 50 mM Tris, pH 8.0).

Luminal Membrane Purification from Mouse Distal Tubular Cell. The luminal membranes from freshly isolated mouse distal tubular cells were purified by using the $MgCl_2$ precipitation technique as described before (28). The tubular cells from the kidneys of 5 animals were pooled in Hanks' buffer and homogenized with a Dounce homogenizer. Following the addition of $MgCl_2$ to a final concentration of 12 mM, the suspensions were stirred on ice for 30 min and centrifuged at 5,000 × *g* for 30 min at 4 °C. The supernatant was collected and centrifuged at 45,000 × *g* for 30 min at 4 °C to precipitate the membranes. The membranes were dissolved in RIPA buffer (150 mM NaCl, 50 mM Tris, pH 7.5, 1 mM EDTA, 0.25% deoxycholic acid, and 1% Nonidet P-40) and assayed for protein expression.

Phos-Tag SDS/PAGE and Phosphatase Treatment. The MDCT cells were lysed in CSK buffer (150 mM NaCl, 1% Triton X-100, 50 mM Tris, pH 8.0). The λ-phosphatase treatment was carried out in the presence of 1 mM $MnCl_2$ and 2 mM DTT according to New England Biolabs' protocol. Phos-tag acrylamide gels were casted by Wako Chemicals. Phos-tag SDS/PAGE was performed in a buffer containing Mn^{++} and Tris-glycine. After electrophoresis, the gel was washed by a buffer containing 10 mM EDTA to remove Mn^{++}, followed by transfer to a PVDF membrane and Western blot. Molecular mass was determined relative to protein markers (BioRad).

The [45]Ca^{2+} Uptake Assay. Radioactive Ca^{2+} uptake levels were determined in vitro in Trpv5-expressing HEK293 cells seeded on poly-L-lysine–coated tissue culture dishes. Cells were pretreated in KHB buffer (110 mM NaCl, 5 mM KCl, 1.2 mM $MgCl_2$, 0.1 mM$CaCl_2$, 10 mM Na-acetate, 2 mM NaH_2PO_4, and 20 mM Hepes [pH 7.5]) supplemented with 25 μM BAPTA-AM for 30 min at 37 °C, washed once with KHB buffer, and incubated for 10 min in KHB buffer at 37 °C. Then, "cold" KHB buffer was aspirated and "hot" KHB buffer containing 1 μCi/mL [45]$CaCl_2$ (PerkinElmer) was added to cells. Voltage-gated Ca^{2+} channel inhibitors (10 μM felodipine and 10 μM verapamil) were included into "hot" KHB buffer to block nonspecific Ca^{2+} conductance. After incubation at 37 °C for 10 min, the reaction was stopped by adding equal volumes of the stop buffer (110 mM NaCl, 5 mM KCl, 1.2 mM $MgCl_2$, 10 mM Na-acetate, 0.5 mM $CaCl_2$, 1.5 mM $LaCl_3$, and 20 mM Hepes [pH 7.5]), followed by extensive washes with the stop buffer. The cells were lysed with the RIPA buffer (150 mM NaCl, 50 mM Tris [pH 7.5], 1 mM EDTA, 0.25% deoxycholic acid, and 1% Nonidet P-40). The radiation level, expressed as disintegrations per minute (dpm), was determined for each cell lysate by using a Beckman 3801 scintillation counter. The protein concentration in each cell lysate was measured with the Bio-Rad protein assay kit and used to normalize the radiation level for each sample, expressed as dpm per microgram protein.

Electrophysiological Recordings. Whole-cell patch-clamp pipettes were pulled from borosilicate glass (Dagan) and had resistance between 1.5 and 3 MΩ. The external solution contains (in mM): 140 Na-gluconate, 10 NaCl, 1 EDTA, 10 glucose, and 10 Hepes (pH 7.4 w/NaOH). Pipettes were filled with (in mM): 140 Na-gluconate, 10 NaCl, 10 EDTA, and 10 Hepes (pH 7.4 w/NaOH). Cells were transfected with 400 ng of TRPV5-GFP and 2.6 μg of wildtype or T303E mutant claudin-16 using Lipofectamine 2000 (Life Technology). In each experiment, the total amount of plasmid DNA for transfection was balanced by empty vector. Current densities were obtained by normalizing current amplitude (obtained at −150 mV) to cell capacitance. Whole-cell recordings were obtained with a low-pass filter set at 2 kHz using an 8-pole Bessel filter in the clamp amplifier. Data were sampled every 0.1 ms with a Digidata-1440A interface.

Cell Membrane Biotinylation. HEK293 cells transfected with claudin-16 and Trpv5 were incubated with 0.25 mg/mL Sulfo-NHS-SS-Biotin (Pierce) in 1× PBS on ice for 30 min. The 50 mM Tris (pH 8.0) buffer was used to stop the biotinylation reaction, followed by centrifugation at 5,000 × *g*. The pellet was dissolved in CSK buffer (150 mM NaCl, 1% Triton X-100, 50 mM Tris, pH 8.0, and protease inhibitors) to extract membrane proteins. The membrane extract was incubated with Neutravidin Agarose (Pierce) to bind biotinylated proteins. The Neutravidin-bound biotinylated proteins were eluted using

Laemmli 2× buffer containing β-mercaptoethanol, followed by SDS/PAGE under denaturing conditions and Western blot.

Coimmunoprecipitation. HEK293 cells expressing GFP-CLDN16 with Flag-Trpv5 or with Myc-ZO-1 were lysed in a hypotonic buffer of 50 mM Tris (pH 8.0) by 25 to 30 repeated passages through a 28-gauge needle, followed by centrifugation at 5,000 × *g*. The membranes of lysed cells were extracted using CSK buffer (150 mM NaCl, 1% Triton X-100, 50 mM Tris, pH 8.0, and protease inhibitors). The membrane extract was precleared by incubation with protein A/G-Sepharose (Sigma-Aldrich) prior to coimmunoprecipitation. The precleared membrane extract was incubated for 16 h at 4 °C with anti-GFP, anti-Flag, anti-Myc, and mouse IgG antibodies. Antibody-bound material was pelleted with protein A/G-Sepharose, washed 3 times with CSK buffer, and detected by immunoblotting.

Protein Electrophoresis and Immunoblotting. Protein concentration in CSK or RIPA buffer was measured by the method of Bradford (Bio-Rad). Protein concentration in Laemmli 2× buffer was estimated based upon the weight of cell pellet according to the following formula (protein weight = 20% of total cell pellet weight). Cell lysates (containing 0.3 to 25 μg of proteins depending upon the biochemical extraction protocol) from cultured cells or isolated distal tubules were subjected to SDS/PAGE under denaturing conditions and transferred to a PVDF membrane, followed by blocking with 3% BSA, incubation with primary antibodies (diluted 1:1,000) and horseradish peroxidase-labeled secondary antibody (diluted 1:5,000), and exposure to an ECL Hyperfilm (Amersham). Molecular mass was determined relative to protein markers (Bio-Rad).

Y2H Protein Direct Interaction Assay. Membrane Y2H direct interaction studies were performed as described before (31). In short, yeast strain NMY51 was transformed with 1.5 μg bait vectors (CLDN16 wt/mutants). Following verification of correct expression and topology of the bait, the upper limit of selection stringency of the baits was determined by using selective double dropout medium lacking leucine, tryptophan, and histidine (SD-LWH). After this step, the yeast strains expressing the bait proteins were transformed with 1.5 μg prey vector (TRPV5). Transformed yeast cells were plated on selective dropout media lacking leucine and tryptophan and incubated for growth of positive transformants. Next, 3 to 6 independent positive transformants were selected and resuspended in 50 mL 0.9% NaCl buffer; 5 μL of each suspension was spotted on SD-LWH medium. Growth of colonies on the selective medium was scored as positive interaction. Quantitative measurements of β-galactosidase activity was performed by lysing 1 mL of 2 OD units each of the overnight culture with 0.05 M Tris, 1% SDS (pH 8.8), and ∼100 μL acid-washed glass beads (Sigma-Aldrich), followed by 3 freeze/thaw cycles in liquid nitrogen. The lysate was incubated for 30 min with 10 μL 10% X-Gal (Carl Roth). Color development was measured by using a spectrophotometer and scored as an indicator of interaction strength. Blank measurements were performed with yeast cells transformed with Claudin-16 (wt) and empty prey vector.

Immunolabeling and Confocal Microscopy. Cells grown on coverslips were fixed with 1% paraformaldehyde in 1× PBS. Mouse kidneys were perfused with 4% paraformaldehyde in 1× PBS, sectioned with a cryostat, and post-fixed with 4% paraformaldehyde in 1× PBS, followed by blocking with PBS containing 10% FBS and incubation with primary antibodies (diluted 1:300) and FITC- or rhodamine-labeled secondary antibodies (diluted 1:200). After washing with PBS, slides were mounted with Mowiol (CalBiochem). Epifluorescence images were collected with a Nikon 80i photomicroscope equipped with a DS-Qi1Mc digital camera. Confocal analyses were performed by using the Nikon TE2000 confocal microscopy system equipped with Plan Neofluar ×40 (NA 1.3 oil) and ×63 (NA 1.4 oil) objectives and krypton-argon laser (488 and 543 lines). For the dual imaging of FITC and rhodamine, fluorescence images were collected by exciting the fluorophores at 488 nm (FITC) and 543 nm (rhodamine) with argon and HeNe lasers, respectively. Emissions from FITC and rhodamine were detected with the bandpass FITC filter set of 500 to 550 nm and the long-pass rhodamine filter set of 560 nm, respectively. All images were converted to TIFF format and arranged using Photoshop CC 2017 (Adobe).

Statistical Analyses. The significance of differences between groups was tested by ANOVA (Statistica 6.0; Statsoft). When the all-effects *F* value was significant ($P < 0.05$), post hoc analysis of differences between individual groups was made with the Newman–Keuls test. Values were expressed as mean ± SEM unless otherwise stated.

ACKNOWLEDGMENTS. We thank Dr. Beate Lanske from Harvard Medical School for kindly providing the Ksp-Cre/PTH1R$^{fl/fl}$ mouse strain. We thank Dr. Krzysztof Hyrc from Washington University Medical School for help with this project. We thank the Washington University Radiation Safety Office for help with [45]Ca^{++} measurement. This work was supported by National Institute of Diabetes and Digestive and Kidney Diseases (NIDDK) Grants R03DK111776 and P30DK079328 (M.T.F.W.), Children's Health System, Dallas (M.T.F.W.), and NIDDK grant R01DK084059 (J.H.).

1. M. F. Michelis, A. L. Drash, L. G. Linarelli, F. R. De Rubertis, B. B. Davis, Decreased bicarbonate threshold and renal magnesium wasting in a sibship with distal renal tubular acidosis. (Evaluation of the pathophysiological role of parathyroid hormone). *Metabolism* **21**, 905–920 (1972).
2. D. B. Simon *et al*., Paracellin-1, a renal tight junction protein required for paracellular Mg2+ resorption. *Science* **285**, 103–106 (1999).
3. J. Hou, M. Rajagopal, A. S. Yu, Claudins and the kidney. *Annu. Rev. Physiol.* **75**, 479–501 (2013).
4. S. Tsukita, M. Furuse, M. Itoh, Multifunctional strands in tight junctions. *Nat. Rev. Mol. Cell Biol.* **2**, 285–293 (2001).
5. J. Hou *et al*., Transgenic RNAi depletion of claudin-16 and the renal handling of magnesium. *J. Biol. Chem.* **282**, 17114–17122 (2007).
6. J. G. Hoenderop *et al*., Molecular identification of the apical Ca2+ channel in 1, 25-dihydroxyvitamin D3-responsive epithelia. *J. Biol. Chem.* **274**, 8375–8378 (1999).
7. J. G. Hoenderop *et al*., Renal Ca2+ wasting, hyperabsorption, and reduced bone thickness in mice lacking TRPV5. *J. Clin. Invest.* **112**, 1906–1914 (2003).
8. K. Y. Renkema *et al*., TRPV5 gene polymorphisms in renal hypercalciuria. *Nephrol. Dial. Transplant.* **24**, 1919–1924 (2009).
9. A. Oddsson *et al*., Common and rare variants associated with kidney stones and biochemical traits. *Nat. Commun.* **6**, 7975 (2015).
10. S. Weber *et al*., Novel paracellin-1 mutations in 25 families with familial hypomagnesemia with hypercalciuria and nephrocalcinosis. *J. Am. Soc. Nephrol.* **12**, 1872–1881 (2001).
11. D. Müller *et al*., A novel claudin 16 mutation associated with childhood hypercalciuria abolishes binding to ZO-1 and results in lysosomal mistargeting. *Am. J. Hum. Genet.* **73**, 1293–1301 (2003).
12. D. Chabardès-Garonne *et al*., A panoramic view of gene expression in the human kidney. *Proc. Natl. Acad. Sci. U.S.A.* **100**, 13710–13715 (2003).
13. J. Hou, D. L. Paul, D. A. Goodenough, Paracellin-1 and the modulation of ion selectivity of tight junctions. *J. Cell Sci.* **118**, 5109–5118 (2005).
14. R. B. Doctor, J. Chen, L. L. Peters, S. E. Lux, L. J. Mandel, Distribution of epithelial ankyrin (Ank3) spliceoforms in renal proximal and distal tubules. *Am. J. Physiol.* **274**, F129–F138 (1998).
15. P. Ronco *et al*., Physiopathologic aspects of tamm-horsfall protein: A phylogenetically conserved marker of the thick ascending limb of henle's loop. *Adv. Nephrol. Necker. Hosp.* **16**, 231–249 (1987).
16. M. D. Lalioti *et al*., Wnk4 controls blood pressure and potassium homeostasis via regulation of mass and activity of the distal convoluted tubule. *Nat. Genet.* **38**, 1124–1132 (2006).
17. F. A. Gesek, P. A. Friedman, Mechanism of calcium transport stimulated by chlorothiazide in mouse distal convoluted tubule cells. *J. Clin. Invest.* **90**, 429–438 (1992).
18. E. Kinoshita-Kikuta, Y. Aoki, E. Kinoshita, T. Koike, Label-free kinase profiling using phosphate affinity polyacrylamide gel electrophoresis. *Mol. Cell. Proteomics* **6**, 356–366 (2007).
19. C. M. Van Itallie *et al*., Phosphorylation of claudin-2 on serine 208 promotes membrane retention and reduces trafficking to lysosomes. *J. Cell Sci.* **125**, 4902–4912 (2012).
20. B. Nilius *et al*., Modulation of the epithelial calcium channel, ECaC, by intracellular Ca2+. *Cell Calcium* **29**, 417–428 (2001).
21. T. de Groot *et al*., Parathyroid hormone activates TRPV5 via PKA-dependent phosphorylation. *J. Am. Soc. Nephrol.* **20**, 1693–1704 (2009).
22. R. Vennekens *et al*., Permeation and gating properties of the novel epithelial Ca(2+) channel. *J. Biol. Chem.* **275**, 3963–3969 (2000).
23. R. Vennekens *et al*., Pore properties and ionic block of the rabbit epithelial calcium channel expressed in HEK 293 cells. *J. Physiol.* **530**, 183–191 (2001).
24. M. T. Wolf, S. W. An, M. Nie, M. S. Bal, C. L. Huang, Klotho up-regulates renal calcium channel transient receptor potential vanilloid 5 (TRPV5) by intra- and extracellular N-glycosylation-dependent mechanisms. *J. Biol. Chem.* **289**, 35849–35857 (2014).
25. M. T. Wolf, X. R. Wu, C. L. Huang, Uromodulin upregulates TRPV5 by impairing caveolin-mediated endocytosis. *Kidney Int.* **84**, 130–137 (2013).
26. B. Nilius *et al*., Whole-cell and single channel monovalent cation currents through the novel rabbit epithelial Ca2+ channel ECaC. *J. Physiol.* **527**, 239–248 (2000).
27. Y. Gong *et al*., The Cap1-claudin-4 regulatory pathway is important for renal chloride reabsorption and blood pressure regulation. *Proc. Natl. Acad. Sci. U.S.A.* **111**, E3766–E3774 (2014).
28. D. Lajeunesse, M. G. Brunette, The hypocalciuric effect of thiazides: Subcellular localization of the action. *Pflugers Arch.* **417**, 454–462 (1991).

29. N. Himmerkus *et al*., Salt and acid-base metabolism in claudin-16 knockdown mice: Impact for the pathophysiology of FHHNC patients. *Am. J. Physiol. Renal. Physiol.* **295**, F1641–F1647 (2008).
30. J. Loffing *et al*., Distribution of transcellular calcium and sodium transport pathways along mouse distal nephron. *Am. J. Physiol. Renal. Physiol.* **281**, F1021–F1027 (2001).
31. J. Hou *et al*., Claudin-16 and claudin-19 interact and form a cation-selective tight junction complex. *J. Clin. Invest.* **118**, 619–628 (2008).
32. T. T. Lambers, R. J. Bindels, J. G. Hoenderop, Coordinated control of renal Ca2+ handling. *Kidney Int.* **69**, 650–654 (2006).
33. P. Ureña *et al*., Parathyroid hormone (PTH)/PTH-related peptide receptor messenger ribonucleic acids are widely distributed in rat tissues. *Endocrinology* **133**, 617–623 (1993).
34. T. Sato *et al*., Parathyroid hormone controls paracellular Ca^{2+} transport in the thick ascending limb by regulating the tight-junction protein Claudin14. *Proc. Natl. Acad. Sci. U.S.A.* **114**, E3344–E3353 (2017).
35. J. Hou *et al*., Claudin-16 and claudin-19 interaction is required for their assembly into tight junctions and for renal reabsorption of magnesium. *Proc. Natl. Acad. Sci. U.S.A.* **106**, 15350–15355 (2009).
36. M. Konrad *et al*., CLDN16 genotype predicts renal decline in familial hypomagnesemia with hypercalciuria and nephrocalcinosis. *J. Am. Soc. Nephrol.* **19**, 171–181 (2008).
37. P. J. Kausalya *et al*., Disease-associated mutations affect intracellular traffic and paracellular Mg2+ transport function of Claudin-16. *J. Clin. Invest.* **116**, 878–891 (2006).
38. K. T. Kahle *et al*., Paracellular Cl- permeability is regulated by WNK4 kinase: Insight into normal physiology and hypertension. *Proc. Natl. Acad. Sci. U.S.A.* **101**, 14877–14882 (2004).
39. K. Yamauchi *et al*., Disease-causing mutant WNK4 increases paracellular chloride permeability and phosphorylates claudins. *Proc. Natl. Acad. Sci. U.S.A.* **101**, 4690–4694 (2004).
40. M. Konrad *et al*., Mutations in the tight-junction gene claudin 19 (CLDN19) are associated with renal magnesium wasting, renal failure, and severe ocular involvement. *Am. J. Hum. Genet.* **79**, 949–957 (2006).
41. A. Ikari *et al*., Phosphorylation of paracellin-1 at Ser217 by protein kinase A is essential for localization in tight junctions. *J. Cell Sci.* **119**, 1781–1789 (2006).
42. D. Günzel *et al*., Claudin-16 affects transcellular Cl- secretion in MDCK cells. *J. Physiol.* **587**, 3777–3793 (2009).
43. A. S. Yu, S. C. Hebert, B. M. Brenner, J. Lytton, Molecular characterization and nephron distribution of a family of transcripts encoding the pore-forming subunit of Ca2+ channels in the kidney. *Proc. Natl. Acad. Sci. U.S.A.* **89**, 10494–10498 (1992).
44. J. M. Anderson, C. M. Van Itallie, Physiology and function of the tight junction. *Cold Spring Harb. Perspect. Biol.* **1**, a002584 (2009).
45. P. J. Chu, H. M. Robertson, P. M. Best, Calcium channel gamma subunits provide insights into the evolution of this gene family. *Gene* **280**, 37–48 (2001).
46. Y. Wei *et al*., The transient receptor potential channel, vanilloid 5, induces chondrocyte apoptosis via Ca2+ CaMKII-dependent MAPK and Akt/mTOR pathways in a rat osteoarthritis model. *Cell. Physiol. Biochem.* **51**, 2309–2323 (2018).
47. O. Andrukhova *et al*., FGF23 promotes renal calcium reabsorption through the TRPV5 channel. *EMBO J.* **33**, 229–246 (2014).